ADVANCED FUNCTIONAL MATERIALS
www.afm-journal.de

Fermi Level Pinning and Orbital Polarization Effects in Molecular Junctions: The Role of Metal Induced Gap States

Colin Van Dyck, Victor Geskin, and Jérôme Cornil*

Understanding the alignment of molecular orbitals and corresponding transmission peaks with respect to the Fermi level of the electrodes is a major challenge in the field of molecular electronics. In order to design functional devices, it is of utmost importance to assess whether controlled changes in the electronic structure of isolated compounds are preserved once they are inserted in the molecular junctions. Here, light is shed on this central issue by performing density functional theory calculations on junctions including diarylethene-based molecules. It is demonstrated that the chemical potential equalization principle allows to rationalize the existence or not of a Fermi level pinning (i.e., same alignment in spite of a varying ionization potential in the isolated compounds), pointing to the essential role played by metal induced gap states (MIGS). It is further evidenced that the degree of level pinning is intimately linked to the degree of orbital polarization when a bias is applied between the two electrodes.

1. Introduction

Molecular electronics offers a totally new paradigm to create electronic devices at the nanoscale.[1,2] Since the pioneering concept of molecular rectifiers introduced by Aviram and Ratner,[3] much progress has been made to create and characterize molecular junctions in a reproducible way.[2,4–7] The field has also benefited from theoretical modelling to rationalize the relationship between the electronic properties of isolated molecules and their transport properties in molecular junctions. State-of-the-art calculations are typically performed in the coherent regime,[8] using a non-equilibrium Green's function (NEGF) formalism coupled to density functional theory (DFT).[2,9–11] Whereas a deep fundamental knowledge has been obtained on molecular junctions including model systems (such as saturated and conjugated chains of increasing length),[4,12] much has still to be learned to define design rules to fabricate functional devices, i.e., exhibiting for instance a high rectification ratio or a high modulation of the current by molecular switching.[7,13] Here, a central issue is to assess the mechanisms controlling the alignment of the electronic levels of the molecule versus the Fermi level of the electrodes in the junction and whether the modulation of the electronic properties of isolated molecules by changes in their chemical structure (for instance via the attachment of electroactive substituents) is retained once the molecules are inserted in the junction.

In this context, we have recently investigated at a theoretical level photoswitching single molecular junctions[14,15] based on a diarylethene photochromic core,[16] see chemical structure in **Figure 1**; the choice of this switching unit was initially motivated by its frequent use in corresponding experimental studies.[17] This molecule exhibits a fully conjugated isomer (closed form, see Figure 1) which can be reversibly photoswitched to a less conjugated twisted isomer (open form, see Figure 1), with a concomitant increase by about two orders of magnitude of the molecular resistance. A key feature coming out of these calculations is that the attachment of electroactive substituents on the photochromic core (see Figure 1) does change significantly the energy of the HOMO level of the isolated molecule while preserving the topology of the orbital along the backbone (see Figure 1) but does not change the alignment of the HOMO level with respect to the Fermi level of the gold electrodes in the junction. In this study, the molecule was directly chemisorbed on the two gold electrodes via a sulphur atom lying on top of a gold atom of the flat (111) surface. When dealing with metal/semiconductor (M/S)[18,19] or metal/organic interfaces (M/O),[20] this effect is usually referred to as a Fermi level pinning. The variation of the level alignment between the HOMO of the molecule and the Fermi level of gold when modulating the chemical structure of the conjugated backbone is typically characterized by a so-called *S*-parameter, that we can define here as:

$$S = \left| \frac{d(E_F - E_{HOMO})}{d(IP_{isolated})} \right| \quad (1)$$

where (E_F–E_{HOMO}) is the energy difference between the Fermi level and the HOMO level of the molecule *in the junction* (level alignment) while IP refers to the ionization potential of the *isolated* molecule. This potential corresponds within exact Kohn-Sham DFT to the HOMO level energy;[21] the latter is naturally subject to the approximate treatment of the exchange-correlation functional but remains a physically meaningful quantity in DFT. When the S-parameter is close to zero, see **Figure 2**, the alignment is independent of the IP of the isolated molecule; this corresponds to the Fermi level pinning regime observed in our previous work.[15] The other extreme, theoretically referred

Dr. C. Van Dyck, Dr. V. Geskin,
Dr. J. Cornil
Laboratory for Chemistry of Novel Materials
20, place du parc, 7000, Mons, Belgium
E-mail: Colin.VanDyck@umons.ac.be

DOI: 10.1002/adfm.201400809

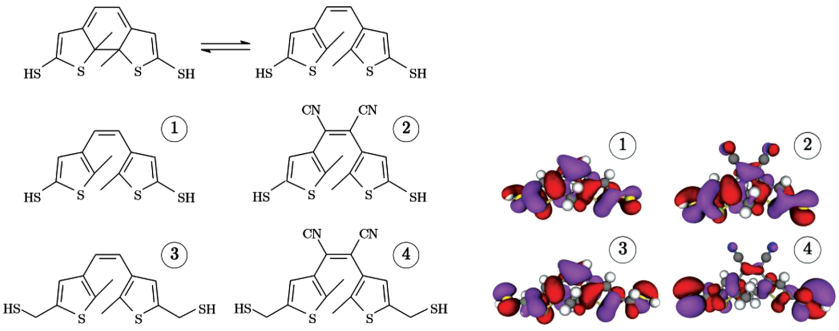

Figure 1. (Left) chemical structures of the diarylethene derivatives under study. Top) Closed and open isomers of the bare photochromic core substituted by thiol linkers; Bottom) Diarylethene derivatives introducing the cyano substituents and/or the saturated spacer. We display on the right side the shape of the HOMO level of the four open isomers involved in our study, as computed at the DFT/GGA.revPBE level within the ATK 2008.10 package.

to as the Schottky-Mott limit, is an S-parameter close to one, which is the dependence predicted by assuming a vacuum level alignment of the electrostatic potential at the interface between the gold surface and the molecule, see Figure 2.

In consistency with theoretical models of the Fermi level pinning for both metal/semiconductor and metal/organic interfaces, the formation of an interface dipole is at the origin of the Fermi level pinning effect.[15] Indeed the latter shifts the electrostatic potential in the molecular region and the amount of interfacial charge transfer is modulated

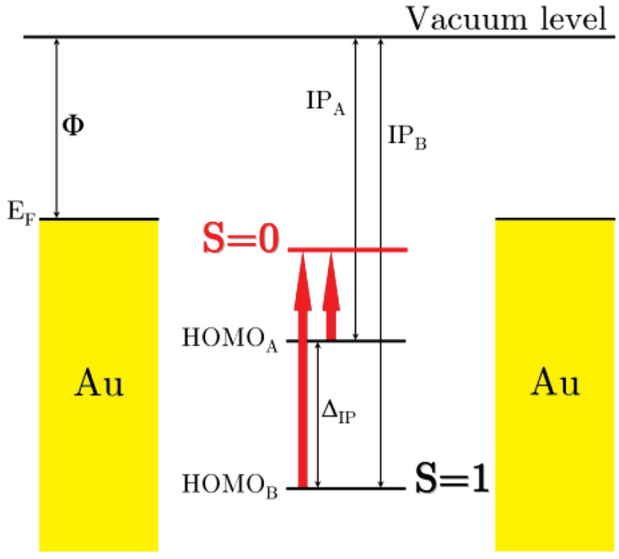

Figure 2. Illustration of both the vacuum level alignment and pinning regimes. Going from species A to B, the ionization potential of the molecule in gas phase is modified by the quantity Δ_{IP}, which corresponds to the denominator of the *S*-parameter in both regimes. According to the vacuum alignment principle, the energy-level alignment with respect to the Fermi level of gold in the junction is also modified by Δ_{IP}; this difference defines the numerator of the *S*-parameter which becomes equal to 1. We illustrate in red the Fermi level pinning regime in which the HOMO level aligns in the same way with the Fermi level whatever the species, the Fermi level alignment is thus unchanged and the *S*-parameter gets equal to zero; note that the shift of the electronic levels is then triggered by the formation of interface dipoles.

such that the alignment is preserved even though the IP of the isolated molecule is shifted with respect to the vacuum level, see Figure 2. Similarly, the Graz group has rationalized the Fermi level pinning effect in chemisorbed self-assembled monolayers by relying on a charge equilibration principle;[22] any deviation from the vacuum alignment regime was attributed in these papers to the fact that the IP of the isolated molecule was located above the Fermi level, thus leading to the formation of an interface dipole via charge equilibration between the metal and the SAM. Actually, this process also occurs when the HOMO level is broadened upon hybridization with the orbitals of the metal and overlaps with the Fermi level though the center of the broadened peak lies below the Fermi level.

Another important effect observed in our previous calculations and in the literature is the spatial localization under bias of the HOMO (initially delocalized in the isolated compound) towards the negative electrode exclusively for the open isomer.[14,15,23] This localization, which we referred to as a polarization effect, leads to the collapse of the corresponding resonant transmission peak under bias due to the lack of electronic density in a part of the molecule and mainly governs the ratio of conductance between the ON (closed form) and OFF (open form) states under bias. Indeed, since the molecular side connected to the positive electrode then becomes an effective tunnel barrier, the polarization reduces the conductance of the open isomer by one order of magnitude, with a similar impact on the On/Off ratio. This also points to the need of relying on a self-consistent treatment of the electronic properties of the junction under bias to provide a reliable description of the I/V characteristics.

In the present contribution, we first aim at rationalizing the transition between the Fermi level pinning and vacuum level alignment regimes from a fundamental chemical potential equalization principle. This is achieved by disentangling the role played by the broadened HOMO level in the junction upon hybridization (characteristic of the HOMO level of the isolated molecule) versus the localized metal induced gap states localized in the vicinity of the interfaces. We will further demonstrate that a polarization effect is only possible in the pinning regime; note that this effect is linker dependent since we observed previously that a conjugation breaking metaphenylene linker was able to significantly reduce the polarization effect.[15] In order to validate these concepts of general applicability, we have considered different diarylethene-based systems represented in Figure 1: (i) the bare photochromic unit in both isomeric forms (the open form is referred as **1** in the following), directly coupled to the gold surface via a thiol functionality; (ii) an open derivative including cyano (CN) substituents on the ethylene bond of the photochromic core (referred as **2** in the following); and (iii) the bare (referred as **3**) and CN substituted (referred as **4**) derivatives introducing a conjugation breaking $-CH_2-$ spacer between the photochromic core and the thiol group.

2. Methodology

We have first optimized the geometries of each isolated molecule of Figure 1 with the Gaussian 2009 package,[24] using a standard DFT/B3LYP/6–31G(d,p) approach,[25] which is known to correctly reproduce the geometries of diarylethene molecules.[26] To ensure that every electronic structure calculation is done at the same level of theory, we have then calculated the electronic levels of the isolated molecule with the ATK 2008.10[9,10] package used for transmission spectra simulations. The GGA.revPBE functional[27] is used in ATK, with a double-zeta + polarization basis set.[28] In a second step, we have contacted the molecules to two semi-infinite gold electrodes, with an on-top geometry of the sulphur atom and a distance of 2.42 Å fixed between the flat (111) gold surface and the sulfur atom, as motivated by previous theoretical and experimental studies.[29] Note that fixing the geometry of the contact is a requirement in our study concentrating on the relationship between IP of the isolated molecule and the final level alignment; as a matter of fact, the alignment is sensitive to the contact geometry and relaxing it would interfere with our analysis of the pinning effect.[30]

The electronic structure and transmission spectra of the junctions are then calculated from the Green's function of the central scattering region, constituted by the molecule and five gold layers on each side. The integration of the Brillouin zone is done with a (7,7,50) Monkhorst-Pack k-sampling.[31] The mesh cut-off for the resolution of Poisson's equation is set to 300 Ry. All these parameters have been carefully tested to ensure the convergence of the transmission spectrum. Naturally, our computational method inherits from the standard DFT limitations also prevailing in many other studies: approximated treatment of the exchange-correlation functional and overinterpretation of the Kohn-Sham energy levels and orbitals.[32] It is known that DFT overestimates the transmission at the Fermi level by less than one order of magnitude compared to experimental data and more sophisticated theoretical approaches, especially when the transmission occurs far from resonance peaks and originates from several transmission channels.[33] The NEGF-DFT approach is nevertheless widely recognized as a robust approach that proves very useful to shed light on a good qualitative basis on new concepts and trends;[6,34,35] this is exactly in this spirit that this approach is used here to examine pinning and polarization effects. Regarding the *S*-parameter defined in Equation (1), whereas the denominator is well reproduced by DFT for isolated compounds in comparison to highly expensive GW calculations,[34] the numerator is governed by the capacity of DFT to predict the proper energy-level alignment. Since the gap is underestimated in DFT at the GGA level, the HOMO level may appear to be too close to the Fermi level, especially in the weak coupling regime[36] which is not addressed in the present study. In our case, the formation of strong covalent Au-S bonds prevents the occurrence of large self-interaction errors and makes the actual gap of the molecule in the isolated state a less critical parameter. Moreover, DFT cannot describe the image charge effects which reduce the gap of molecules adsorbed on metallic surfaces.[37] This limitation compensates to some extent for the gap underestimation,[38] thus rationalizing the relevance of using an NEGF-DFT approach.

In order to identify the orbitals at the origin of the resonant transmission peaks, we rely on the molecular projected self-consistent Hamiltonian (MPSH) method.[10] This consists in diagonalizing the Hamiltonian of the central region, extracted from a self-consistent treatment of the full system with an explicit account of the semi-infinite electrodes, projected in a restricted LCAO basis set, in which only the atoms of the molecule and the first two gold layers on each side of the molecule are involved. We have also characterized the charge reorganization at the interfaces by considering first a model system made of the diarylethene core substituted by a single gold atom on each side and by replacing then the gold atom by gold electrodes; this is done by computing the electronic density of the pristine gold surface, ρ_{gold} and of the molecule perturbed by two gold atoms, $\rho_{mol+2Au}$ compared to the electronic density of the entire system, ρ_{all}, and of a system constituted by the two isolated gold atoms, ρ_{2Au}. We evaluate the plane averaged reorganization, $\delta\rho(z)$, (with z the transport axis), occurring upon replacement of the single gold atoms tethered to the molecules by real electrodes, according to:

$$\delta\rho = \rho_{all} - \rho_{mol+2Au} - \rho_{gold} + \rho_{2Au} \quad (2)$$

This is done for a closed periodic system instead of an open one in order to guarantee charge conservation; in practice, the molecule is sandwiched between two electrodes made of eight gold layers and this unit cell is repeated periodically in three dimensions. The reorganization profile has also been related in our analysis to the profile of the Fukui function, $f(z)$, of the system constituted by the molecule and the two gold atoms.[39] The Fukui function depicts the sensitivity of the chemical potential under an external perturbation and is sometimes referred to as a reactivity index. In our calculations, the neutral Fukui function is approximated, assuming no relaxation of the frontier Kohn-Sham orbitals following a small charge transfer, from the HOMO and LUMO orbitals $\Phi_{HOMO/LUMO}$, as:[39]

$$f(\vec{r}) = \frac{1}{2}\left(\Phi^2_{HOMO}(\vec{r}) + \Phi^2_{LUMO}(\vec{r})\right) \quad (3)$$

3. Results

3.1. Metal Induced Gap States (MIGS) in a Molecular Junction

When different species are interacting, a chemical potential equalization must occur, which is at first sight hard to conciliate with a vacuum level alignment assumption leading to an *S*-parameter of 1, as supported by the trends observed in a recent experimental study.[40] For metal/semiconductor or thick metal/organic interfaces, the conciliation is made possible by a band-bending phenomenon, shifting the electrostatic potential over a space-charge region about a few tens of nanometers in the semiconductor.[19] The spatial scale of this phenomenon is by far too large to be applied to a single molecule in a junction (with a width less than 1.7 nm for our diarylethene molecules).

Table 1. Ionization potentials (IP) of the isolated molecules (calculated as $-\varepsilon_{HOMO}$) and energy offset between the midgap value of the isolated molecules and the Fermi level of gold (referred to as MGA: MidGap Alignment). The last line contains the variation in IP and MGA when attaching the CN electroactive substituents while the last column describes the variation in IP and MGA when introducing the saturated spacer.

	–SH	$-CH_2SH$	Δ
–H	IP = –4.73 eV	IP = –4.65 eV	+0.08 eV
	MGA = –1.67 eV	MGA = –1.65 eV	+0.02 eV
–CN	IP = –5.28 eV	IP = –5.02 eV	+0.26 eV
	MGA = –1.19 eV	MGA = –1.08 eV	+0.11 eV
Δ	–0.55 eV	–0.37 eV	
	+0.48 eV	+0.57 eV	

Indeed, any change in the electrostatic potential induced at the surface by the adsorption of molecules is screened in the metal and does not extend beyond a single gold layer,[41] thus justifying the inclusion of a limited number of gold layers in the scattering region. Without a space-charge region of large dimension, the vacuum level alignment assumption is thus a static assumption neglecting any equilibrating charge transfer.

We report in **Table 1** the IPs of the isolated species described in Figure 1, as computed from the HOMO level energy. All compounds display a HOMO level delocalized over the conjugated core and exhibiting the same nodal structure, see Figure 1. The HOMO energy is insensitive (i.e., no modification in the IP) to the addition of the saturated spacer as expected from its π-character. Thus, within a vacuum level alignment regime, we do not expect any difference in the level alignment with or without the saturated linker. On the other hand, for both linkers, the electron withdrawing -CN substitution significantly stabilizes the HOMO level (i.e., increase in the IP). A vacuum level alignment regime would thus promote a very different alignment in the junction. This principle contrasts with the previously observed pinning effect associated to the formation of interface dipoles.[15] We observed that these dipoles have an amplitude which correlates with the modification of the chemical potential, μ, of the isolated molecules upon attachment of electroactive substituents. The chemical potential of the isolated molecule can be evaluated from the midgap value: $\mu = -(IP+EA)/2$, where EA is the electron affinity of the system typically associated to the LUMO level. Actually, using DFT as an exact theoretical framework,[39] it has been rigorously demonstrated that the chemical potential is nothing else than opposite sign of the Mulliken electronegativity of the molecule,[42,43] which is a concept used for decades in chemistry together with an equalization principle.[43,44]

Figure 3 displays the transmission spectrum at equilibrium for the four open isomers. The introduction of a saturated linker clearly modifies the alignment mechanism. The intense resonant peak associated to **1** is shifted down by about 0.75 eV by the incorporation of a saturated spacer (**3**) while the IPs of the isolated compounds only differ by 0.08 eV. Moreover, the spacer also appears to prevent Fermi level pinning since a further shift down of the transmission peak by about 0.27 eV is observed when introducing CN on the photochromic core (going from **3** to **4**). In all cases, analysis of the MPSH spectrum indicates that the first resonance peak still originates from the level having the same shape as the HOMO orbital of the isolated compounds, see Figure 1. From these calculations, we can estimate an *S*-parameter around $S \approx \Delta(E_F - E_{HOMO})/\Delta IP = 0.27/0.37 = 0.73$ with the saturated spacer while it is estimated to be around $S \approx 0.05/0.55 = 0.09$ without it. This clearly demonstrates that the vacuum alignment principle fails in describing the significant role of the saturated spacer.

The same conclusions hold true when considering a naive chemical potential/electronegativity equalization through a direct alignment of the chemical potential of the isolated species with the gold Fermi level (in practice, by setting the midgap of the molecule at the Fermi level of the electrodes). We refer to this principle as the midgap alignment (MGA). According to it, the energy difference between the electrode Fermi level and the HOMO orbital in the junction is given by the energy gap between the midgap and the ionization potential of the isolated species: MGA = |μ–IP|. This principle, sometimes referred to as electronegativity equalization method, has already been applied

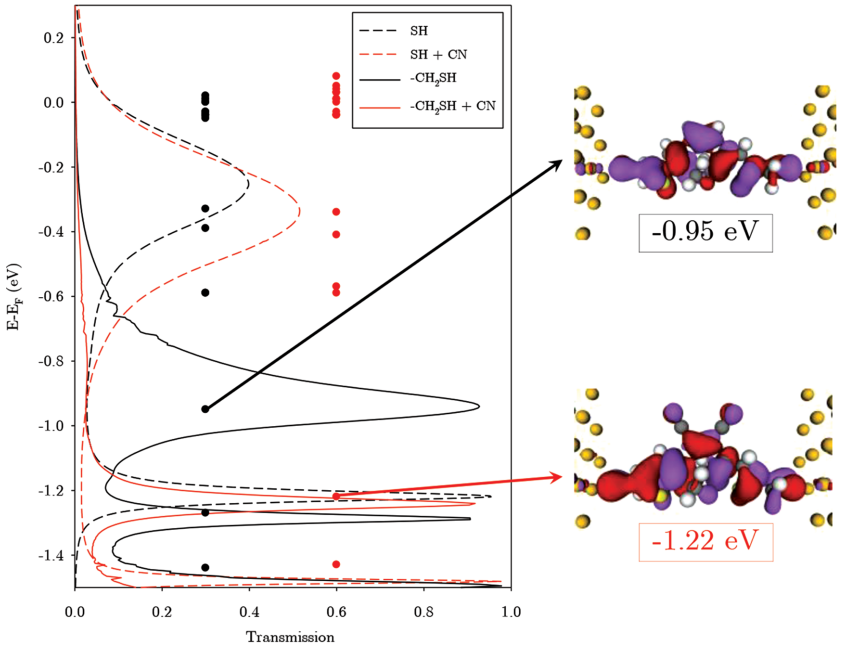

Figure 3. Transmission spectra of the open isomers **1–4**. The black and red dots correspond to the MPSH orbital energies of the unsubstituted and CN-substituted open isomer in presence of the saturated linker. We illustrate on the right side the shape of the MPSH orbitals (other levels correspond to orbitals localized on the electrodes) associated to the first transmission peak for the structures including the saturated spacer, showing the signature of the HOMO level of the isolated compound, as reported in Figure 1.

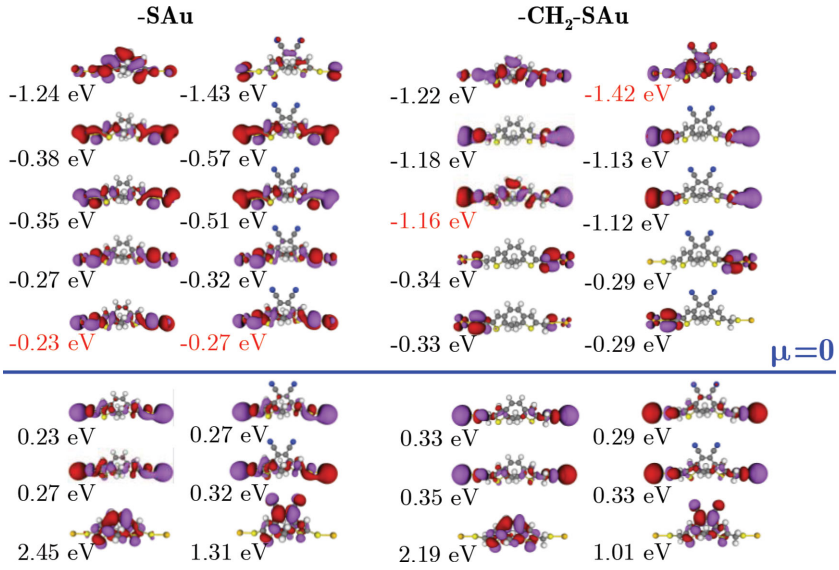

Figure 4. Frontier molecular orbitals of the open isomers **1–4** when replacing the hydrogen atoms of the thiol groups by single gold atoms on each side of the molecule. The midgap energy has been set to zero. We highlight in red the energy values of the first occupied orbital exhibiting the signature of the HOMO level of the isolated compound, in comparison to the HOMO of the unsubstituted molecule given in Figure 1.

in other works to compute partial atomic charges,[45] metal/semiconductor or metal/organic interface dipoles[19,46] or partial charges for redox complexes in molecular junctions.[47] On that basis, we cannot clearly rationalize the pinning effect going from **1** to **2** or the apparent strong impact of the saturated spacer, as evidenced from the variation of the MGA parameter when introducing -CN substituents or a saturated linker (ΔMGA, which should correspond to the numerator of the S-parameter in Equation (1)), see Table 1. The chemical potential of the isolated compounds, with a thiol group (-SH) on each side, cannot thus be exploited to predict the final alignment in the molecular junction.

Within the DFT framework, it has been shown that the change in the chemical potential $d\mu$ of a system by a small external perturbation of the total charge, dN, and external potential, δv, is given by:[39]

$$d\mu = \eta dN + \int f(r)\delta v(r)dr \quad (4)$$

where η is the hardness and f the Fukui function. When the molecule is attached to the gold electrodes, a charge reorganization, $\delta\rho$, is promoted to equalize the chemical potential of the molecule with the gold Fermi level. According to Equation (4), this can be achieved in two ways: (i) the charge reorganization generates a net charge on the molecule, modifying its chemical potential as a function of the hardness parameter; (ii) the whole electronic reorganization creates a perturbation of the external potential which modifies the chemical potential according to the Fukui function of the molecule. The charge reorganization profile, $\delta\rho$, must then be closely connected to this equation. However, the bonding of a thiol to a gold electrode is far from being a small perturbation of the isolated species. This suggests that considering the isolated species undergoing the gold perturbation is irrelevant to rationalize the alignment process in terms of chemical potential equalization. In order to characterize the interfacial charge reorganization, we have thus considered an intermediate isolated reference system (i.e., not inserted between gold electrodes), in which the two hydrogen atoms of the thiol groups (SH) in the molecule are substituted by two single gold atoms on each side (SAu). We will show in the following that it is meaningful for our analysis to consider this relatively slightly perturbed system, prior to analyzing the full system comprising the gold electrodes.

Figure 4 illustrates the shapes and energies of the frontier electronic levels of the four open isomers perturbed by the two gold atoms. When a saturated linker is present, the HOMO of the perturbed system does not show any remaining signature of the delocalized HOMO orbital of the isolated molecule (Figure 1) and is actually localized in the vicinity of the interface on the gold and sulphur atoms; the first delocalized orbital, exhibiting the same shape as the HOMO level of the isolated molecule (Figure 1), lies much deeper in energy. On the other hand, in presence of the conjugated linker, the hybridized HOMO level includes the signature of the HOMO level of the isolated molecule. These changes in the electronic structure upon introduction of the saturated linker have strong implications. Indeed, when the hybridization with gold induces new localized states inside the energy gap between the highest occupied and lowest unoccupied delocalized π-orbitals in the junction, these metal induced gap states (MIGS), now defines the chemical potential as the midgap of the perturbed system, and drives the alignment process. Since the charge reorganization only occurs between MIGS and the gold electrode due to the weak coupling between the π-conjugated backbone and the anchoring group, the delocalized level characteristic of the HOMO of the isolated molecule is no more involved in the chemical potential equalization process so that there is no reason for this level to be pinned to the Fermi level. This is further reflected in the analysis of the charge reorganization profile reported in **Figure 5**, as done in the next paragraph. Any modification in their absolute energy in the isolated compound is thus well reflected in the transmission spectrum of the full system. This is why the application of the midgap alignment principle based on isolated species in Table 1, i.e., prior to hybridization, cannot reproduce the trends observed in the junction. We have thus identified here the key-role played by metal induced gap states and hybridization in the alignment process. Such MIGS have already been observed in previous theoretical studies since they can induce a low transmission signal around the Fermi level[48] and have also been evidenced in experimental measurements.[49] On the other hand, when the HOMO of the perturbed system still exhibits the signature of the HOMO of the isolated molecule, the conjugated

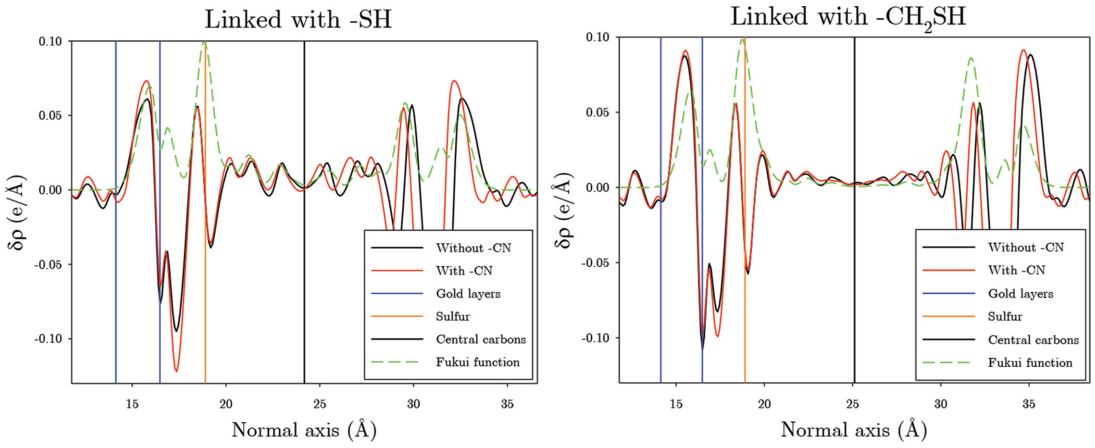

Figure 5. Electron density reorganization when replacing the single gold atoms in the model systems illustrated in Figure 3 by semi-infinite electrodes. We report in dashed green the Fukui function of the model system with single gold atoms and without the CN substituents, integrated over the x,y-coordinates and scaled arbitrarily (i.e., multiplied by a constant) to fit in the graph. The vertical bars point to the position of some reference atoms in the junction.

backbone is involved in the definition of the chemical potential as the midgap of the perturbed molecule which must equalize the gold Fermi level (insensitive to surface changes and associated in good approximation to its chemical potential). Consequently, differences among the IPs of the isolated switches have then to be wiped out by a chemical potential equalization process in the junction.

Perturbing the molecule with two gold atoms is surprisingly a very efficient way to illustrate the alignment process. Indeed, using the midgap alignment principle for the system now substituted and perturbed by two single gold atoms, we can predict an alignment fully consistent with that prevailing with the complete open system calculations (where semi-infinite gold electrodes replace the single gold atoms), as reported in Figure 4 where the chemical potential at midgap has been set to zero. After having identified the first occupied orbital exhibiting the signature of the HOMO of the isolated compound system, the corresponding energy (in red) directly corresponds to the Fermi-level alignment predicted by the midgap alignment principle. For the two perturbed molecules lacking the saturated spacer, this energy is about –0.23 eV for **1** to be compared to –0.27 eV for **2**. This leads to an *S*-parameter of about 0.07 and hence to a pinning regime consistent with the full calculations in Figure 3. When the saturated spacer is introduced, the delocalized orbital shifts down with respect to the midgap and the predicted alignment goes from –1.16 eV in **3** to –1.42 eV in **4** with a CN substitution. This is also consistent with the full calculations and leads to an S-parameter around 0.7 and hence to no pinning effect.

We discussed in the previous paragraphs the role of the MIGS in the alignment process in term of a chemical potential equalization. The latter actually occurs through a charge reorganization process upon connecting the intermediate system to the gold electrodes (i.e., when the single gold atoms are replaced by the semi-infinite electrodes), as described in Figure 5. We observe that this reorganization, defined by Equation (2), takes place over a region encompassing the photochromic core in **1** and **2** whereas it remains localized around the interface with a saturated spacer. In the continuity of the previous considerations, we attribute the contribution or not of the MIGS in the chemical potential equalization as the origin of this difference in localization. We have superimposed in Figure 5 the Fukui function profile for the intermediate system onto the charge reorganization profile. The Fukui function is constructed on the basis of the frontier orbitals, according to Equation (3). We observe a direct correlation between this quantity and the charge reorganization. This shows a clear connection between the electronic structure of the intermediate system and the electronic reorganization taking place to achieve equilibrium. This clear link is due to the fact that our intermediate system includes a sufficient perturbation to observe the creation of MIGS. For systems **1** and **2** featuring a hybridized frontier orbital with a delocalized character, the Fukui function is also delocalized over the photochromic core, thus rationalizing the large extent of the charge reorganization over the photochromic core in Figure 5. On the other hand, in presence of the saturated spacer inducing MIGS, the reactivity, driven by the frontier orbitals (see Equation (3)) that are gap states, is concentrated at the interface. Therefore, to equalize the chemical potential, the perturbation due to charge reorganization must also be exclusively localized at the interface, according to the integral term of Equation (4), as clearly observed in Figure 5 for systems **3** and **4**. This is a second evidence, after the good qualitative trend given by the midgap alignment principle, that the creation of MIGS play a crucial role in the chemical potential equalization process.

Integrating these reorganization profiles given by Equation (2) along the transport axis between the two most external carbon atoms of the molecule gives access to the amount of charge transferred to the molecule when replacing the gold atoms by real electrodes. An excess charge of 0.093|e| is found in **1** and increases up to 0.117|e| upon CN substitution in **2**. In the presence of the saturated linker, the excess charge is practically the same in the two derivatives (0.064|e| in **3** and 0.060|e| in **4**). For both linkers, the CN substitution lowers the chemical potential of the system perturbed by two gold atoms by 0.24 eV. The amount of charge transfer on the central backbone is, however, too small to cope for the evolution of the

chemical potential upon CN substitution through the first term of Equation (4) (the hardness approximated as the DFT gap in Figure 4 is indeed only around 0.5 eV for our studied systems). It is thus the Fukui function present in the second term of Equation (4) which drives the equilibrium in the junction via an amplified charge reorganization, and hence external potential perturbation, at the interface. This explicitly shows that the absolute electron transfer induced by the electrodes on the molecule is less important than the subtle shape of the charge reorganization profile to best characterize the alignment process for molecular junctions with strong gold/sulfur contacts.

3.2. The Role of Pinning in the Polarization Effects

We will describe in this Section how the polarization and pinning effects are related to the structure of the molecule and its bonding to the metal using a qualitative pictorial model that will provide a framework for the analysis and understanding of the theoretical results. To do so, we consider the frontier electronic levels of both the open and closed isomers as built from the orbitals of the three constitutive fragments: two symmetric lateral rings and the bridge, as represented in **Figure 6**. The frontier molecular orbitals get delocalized over the photochromic core through the π-coupling between the two lateral aromatic rings and the conjugated bridge. In the flat closed isomer, the maximized overlap between the p_z orbitals of the conjugated backbone yields a strong coupling between the units whereas the couplings are reduced in the open isomer due to the twisted geometry of the backbone.

We now consider two limiting scenarios once the molecule is sandwiched between the two gold electrodes, see **Figure 7** where we have reported the relevant levels for each individual units (electrodes and fragments):

(i) In the first scenario, we assume that there is no coupling between the lateral fragments and the electrodes, so that no charge transfer and equilibration process between the molecule and the electrodes can take place. When a bias ΔV is applied in the junction with the positive pole on the left electrode, the frontier orbitals of the three fragments shift electrostatically, making the electronic levels of the left fragment more stable than those of the right fragment. This tends to promote a larger localization of the HOMO of the entire molecule on the right lateral fragment, giving rise to a polarization of the orbital. However, due to the internal π-coupling between the units, the natural response of the molecule is to transfer electrons towards the positive side, and hence to generate an electric field counter-balancing the external one and reducing the degree of polarization of the orbitals, see left part of Figure 7.

(ii) The second scenario assumes the absence of internal coupling through the bridge but a strong coupling between the lateral rings and the corresponding electrodes. This allows for charge reorganization at the interface and for the observation of the pinning effect. When the same bias ΔV is applied, the Fermi levels of the electrodes are shifted in energy due to the electrostatic potential as well as the frontier orbitals of the associated isolated fragments though with a smaller amplitude due to their location within the nanogap. In order to recover the alignment at equilibrium imposed by the pinning effect at each interface, a charge transfer must occur under bias, shifting down the energy of the fragment orbitals at the positive electrode and shifting up the fragment orbitals at the negative electrode, see right part of Figure 7. The final electrostatic profile displays a screening of the field at the interface and an amplification of the potential offset between the lateral rings, in contrast to the previous scenario.

The two scenarios also imply charge accumulation in two opposite ways in order to screen (i) or amplify (ii) the electric field in the molecular region, which should make them easily distinguishable. Accordingly, we have computed the electron density profile (integrated in the plan perpendicular to the transport direction) across the molecular junctions and its reorganization under bias as:

$$\delta\rho(z,V) = \rho(z,V) - \rho(z,0) \tag{5}$$

In order to facilitate the analysis, we have plotted the cumulated change of electron density under bias by integration of the profile of Equation (5). We define this quantity as:

$$\delta Q(z,V) = \int_0^z \delta\rho(z',V)\,dz' \tag{6}$$

In such profiles, any increase of $\delta Q(z,V)$ in a given region implies that the electron density increases under bias in that region and vice versa. Interestingly, from the schemes in Figure 7, we expect in the absence of external coupling a convex $\delta Q(z,V)$ profile in the molecular region due to the increased/decreased electron density at the positive/negative sides. On the other hand, we expect a concave profile in the absence of internal coupling since the electron density must decrease/

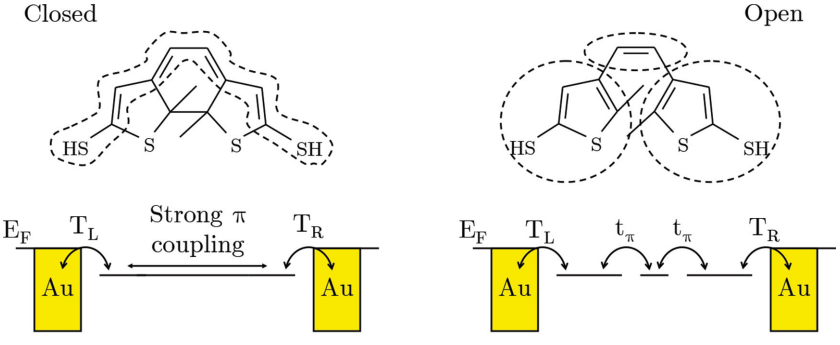

Figure 6. Schematic representation of the HOMO level of the closed and open forms of the bare photochromic unit inserted between the two gold electrodes, with T_L and T_R representing the interfacial coupling. The closed form is characterized by a strong electronic coupling between the three fragments due to its planarity. The open isomer is characterized by a weaker internal coupling (t_π) between the fragments due to the torsion angles introduced within the backbone.

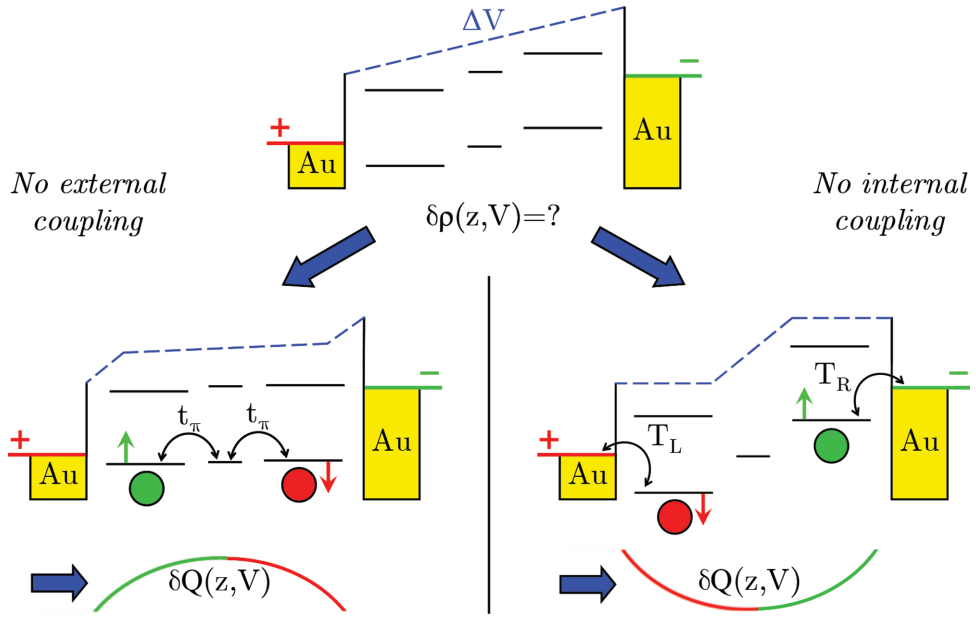

Figure 7. Schemes illustrating the two antagonistic mechanisms occurring under application of a bias between the two electrodes as a function of the strength of interfacial (external) versus internal couplings. The top diagram shows the electronic structure expected for the three individual fragments of the molecule and for the Fermi level of the electrodes when applying a bias with the positive pole on the left electrode. In the absence of external coupling (left), a charge rearrangement takes place to screen the electric field and reduce the polarization effect. In the absence of internal coupling (right), the charge rearrangement occurs to pin the external fragments to their respective electrodes and recover the alignment prevailing without the field. The circles represent the extra amount of positive (in red) or negative (in green) charges required to reach equilibrium. The dashed line depicts the profile of the voltage drop across the junction in the two different scenarios. We depict below the qualitative $\delta Q(z,V)$ concavity profile expected for each scenario.

increase on the left/right fragments to recover the alignment at equilibrium with the left and right electrodes after the field perturbation. Note also that $\delta Q(z,V)$ integrates to zero over the entire molecule without external coupling; its actual value in a junction reflects the charge exchange with the electrodes for a given bias.

Such profiles, obtained by applying 0.9 V through the junction, are reported for both the closed and open isomers of **1** in the left two plots of **Figure 8**. The profile points to a progressive reduction of the electronic density when moving away from the positively charged left electrode, shifting down the levels in energy toward the stabilized positive electrode. The asymmetry of the profile further indicates that a similar pinning to the opposite, destabilized, electrode is hard to achieve in practice. Abstracting this general trend, the profile is found to be convex for the closed isomer while it is concave for the open isomer. In the closed isomer, the internal π-coupling is strong and dominates over the external coupling scenario, so that there is no trend to preserve the pinning but rather to screen the electric field via internal electron transfer from the right side to the left side of the molecule. The concavity for the open isomer is consistent with a strong pinning effect of each lateral fragment due to low internal π-coupling triggered by the torsions along the backbone in the open form. This amplifies the internal electric field and is thus expected to amplify as well the polarization effect.

The corresponding evolution of the MPSH spectrum under bias is shown in **Figure 9** for the open isomer. We clearly see that the energies of the HOMO and HOMO–1 levels evolve in opposite directions under bias, with the HOMO polarized toward the negative destabilized electrode and the HOMO–1 toward the positive stabilized electrode. At a certain bias, the HOMO and HOMO–1 are strongly polarized toward the opposite electrodes, pointing to an energy splitting of the two fragments.

From our previous considerations, we expect that a strong reduction of the pinning effect for the delocalized orbital shown in Figure 1 should also annihilate the polarization effect. This should thus be observed in the presence of a saturated spacer which promotes the creation of MIGS and prevents the delocalized orbital of the molecules to be pinned by the electrodes. Such gap states follow their respective electrodes under bias and lead to charge rearrangements localized at the interface, which do not affect the central photochromic core. **Figure 10** reports the transmission spectrum of the open isomer with a saturated linker under a bias of 0.90 V and 1.05 V (the latter value ensures the same magnitude of the electric field in comparison to a junction with shorter SH linkers under a bias of 0.9 V). For **1**, the polarization effect leads to a collapse of the HOMO transmission peak with a bias of 0.9 V, down to 28% of the intensity at zero volt.[15] When the saturated linker and MIGS are introduced in **3**, the polarization effect is well prevented, with only a small decrease in the peak intensity by 13% compared to the zero-bias intensity. **Figure 11** illustrates the evolution of the MPSH spectrum of **3** under bias. The two gap states are highlighted in orange and follow their respective electrodes while the electronic level featuring the characteristics of the HOMO level of the isolated compound (see Figure 1)

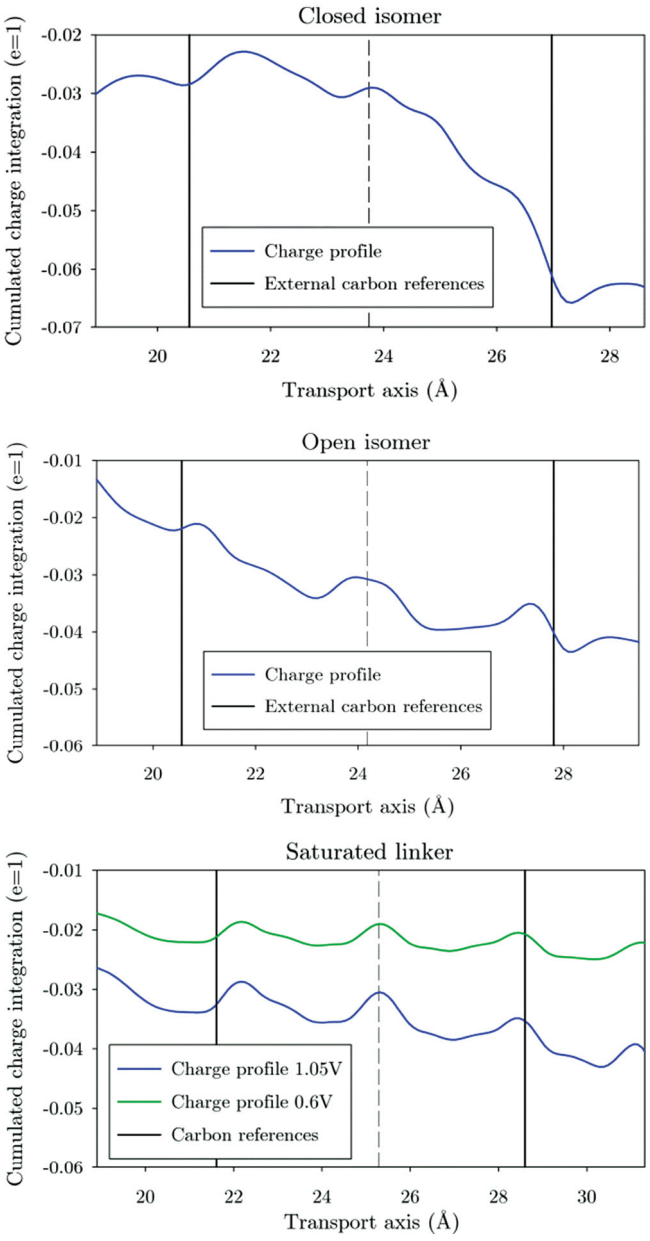

Figure 8. Cumulated integration of the electron density reorganization under a bias of 0.9 V for the closed (left) and open (middle) isomers when replacing the single gold atoms by semi-infinite electrodes; (right) corresponding profiles at 0.6 V and 1.05 V for the open isomer with a saturated linker. The black vertical bars point to the position of the external carbon atoms in the junction.

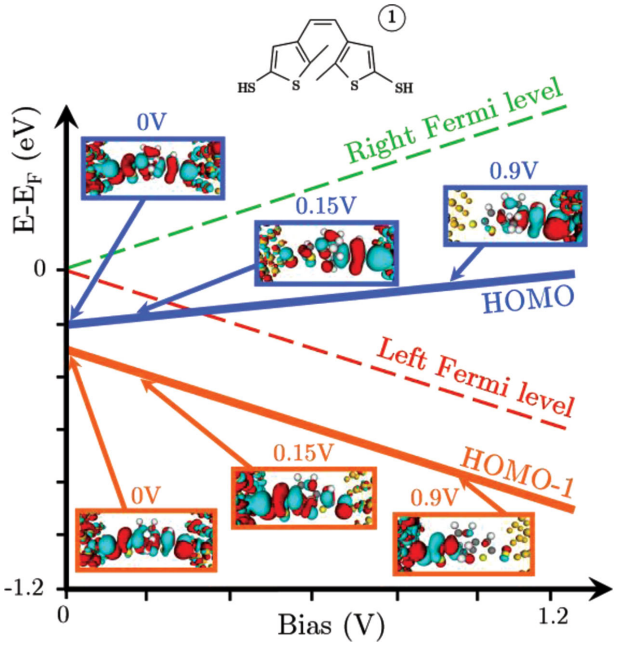

Figure 9. Evolution of selected levels and corresponding orbital shapes under bias on the basis of the MPSH spectrum (as represented in Figure 3 for the equilibrium situation) for the open isomer connected to gold via the sulfur linker. This is extracted from a calculation on the molecule sandwiched between semi-infinite electrodes with an applied bias evolving per step of 0.15 V. The MPSH spectrum includes many levels which is the reason why we replaced it here with a simplified figure on the basis of the full spectra reported in the Supporting Information (Figure 9bis). The dashed lines show the opening of the transmission window under bias. The orbital with a shape similar to the HOMO of the isolated molecule evolves in energy along the blue line and gets polarized towards the negative electrode while the level associated to the HOMO–1 (orange line) gets polarized towards the positive one. Finally, at 0.90 V we reach a situation in which the HOMO and HOMO–1 orbitals can be viewed as the two separate external fragments displayed in Figures 6 and 7.

is highlighted in blue. Under bias, one gap state enters into the transmission window (defined as the gap between the two Fermi levels of the electrodes), and then starts to decay in energy; this is attributed to charge transfer processes towards the electrodes. Below, the second gap state starts mixing with the delocalized orbital when reaching a bias around 0.75 V, marked by a vertical black line. Below this threshold voltage, the delocalized orbital does not get polarized, thus explaining the absence of collapse in the transmission peak. However, the delocalized orbital can possibly take part to the equilibration of the chemical potential beyond that threshold and get polarized; unfortunately, the MPSH analysis shows that the level then results from a mixing between the delocalized orbital and the gap states, preventing any clear conclusion about its actual degree of polarization.

Figure 8 further describes the profile of $\delta Q(z,V)$ upon introduction of the saturated spacer for the open isomer for a bias below and above the threshold value. The profile is flat, with no general decreasing trend when compared to the sulphur linker. This is rationalized by the fact that there is no delocalized orbital for which a pinning to the most stable electrode must be promoted due to the formation of the MIGS. It is also hard to conclude anything concerning a concavity amplifying or screening the electric field since we are in an intermediate situation between the two extreme scenarios due to the weak internal couplings and pinning effects. Interestingly, a bump is observed for the three profiles at the position of the conjugated bridge (double bond between the thiophene rings), pointing to a screening of the electric field in these fully conjugated parts.

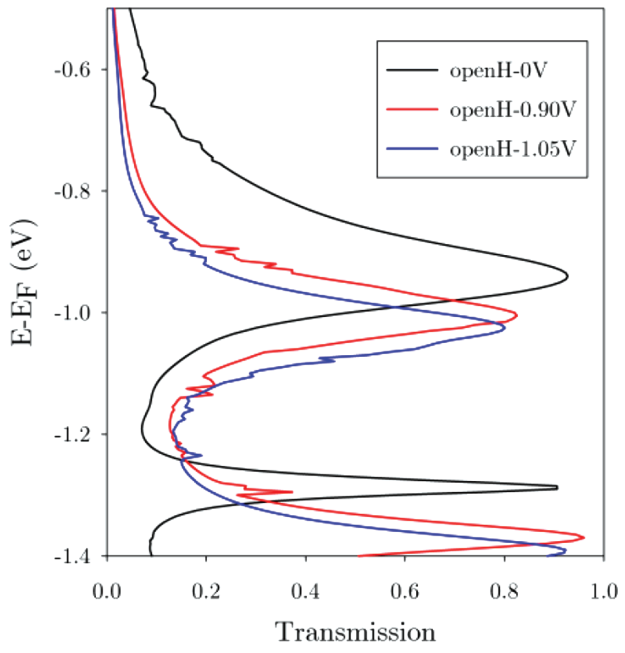

Figure 10. Evolution of the transmission spectrum under bias for the open isomer with a saturated spacer.

4. Conclusions/Synopsis

In this paper, we have investigated the central issue of level alignment in molecular junctions, with diarylethene molecules chosen as a representative case study. We rely on the fundamental principle of chemical potential equalization to rationalize this alignment. The latter is characterized by an *S*-parameter, evolving between 0 (Fermi level pinning) and 1 (vacuum level alignment trend), depending on the degree of changes in the alignment upon modification of the ionization potential of the isolated compounds. We showed that the introduction of a saturated spacer between the photochrome and the gold surface strongly impacts the level alignment; the pinning effect is strongly reduced and *S* can reach values close to 1. In order to shed light on the chemical potential equalization process, we studied the electronic structure of the systems perturbed by two single gold atoms and the way the electronic properties are affected when replacing those single gold atoms by semi-infinite electrodes. When the terminal sulphur atoms are linked to a single gold atom, the molecular orbitals can hybridize with those of gold in two different ways:

(i) the delocalized HOMO of the isolated molecule can hybridize in such a way that the new highest occupied orbital of the hybridized system still carries the signature of the delocalized HOMO level of the isolated compound. The chemical potential of the system is then related to the energy of the delocalized HOMO level in the junction and a change in the ionization potential of the isolated molecule via electroactive substituents is compensated by a charge reorganization at the interface to ensure the equalization principle. This is the pinning regime characterized by $S \approx 0$.

(ii) as observed with the saturated spacer, the hybridization can lead to the creation of states localized at the interface inside the π-orbital gap of the unsubstituted molecule. Metal induced gap states then define the chemical potential and are involved in the chemical potential equalization process. The delocalized HOMO level characteristic of the isolated molecule is then no more involved in the alignment process. This annihilates the Fermi level pinning effect and allows tuning the energy barrier between the Fermi level of the electrodes and the delocalized level in the junction through simple electroactive substitutions. This regime is characterized by $S \approx 1$.

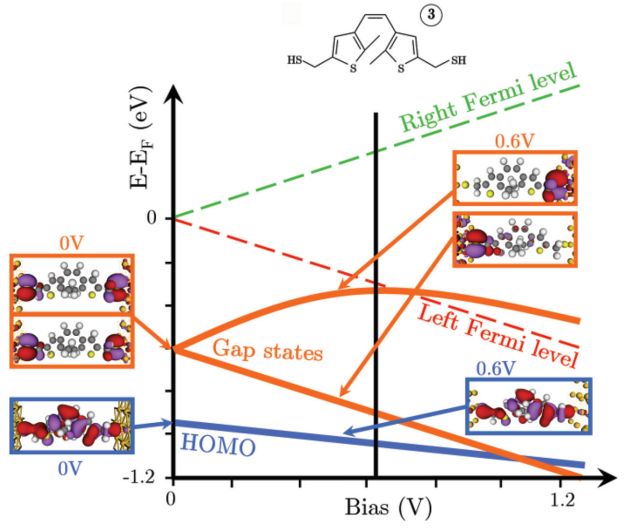

Figure 11. Evolution of selected levels and corresponding orbital shapes under bias on the basis of the MPSH spectrum for the open isomer connected to gold through the -CH_2SH linker. As it is the case for figure 9, it is a simplified figure and the full spectrum is given as Supporting Information (figure 11bis). The two gap states (depicted by the orange lines) follow their respective electrodes under bias (the dashed lines correspond to the Fermi levels of the electrodes) and prevent the HOMO (blue line) to get polarized. Beyond a threshold voltage of 0.75 V (marked as a vertical black line at this bias), the situation becomes more complex when the HOMO level starts mixing with the lowest gap state to generate a hybrid orbital and the highest gap state starts to shift downward.

The relevance of the simple system perturbed by two single gold atoms is demonstrated by the consistency of the *S*-parameters obtained compared to the full system with two semi-infinite electrodes, assuming a midgap alignment process. Moreover, the Fukui function of the simple perturbed system correlates very well with the charge reorganization profile observed when replacing the single gold atoms by real electrodes, as the simple perturbation is sufficient to observe the creation of MIGS.

In a second stage, we have analyzed the factors governing the extent of polarization of the initially delocalized HOMO orbital under bias for the open isomer. Two extreme scenarios have been envisaged: (i) an amplification of the electric field for strong interfacial couplings (i.e., pinning effect); (ii) a screening of the electric field for strong internal π-couplings. The two opposite scenarios can be distinguished by the profile of the cumulated integration of the charge density reorganization induced by the bias. In the open isomer with SH linkers, the interfacial coupling dominates over the internal coupling due to the torsions induced along the conjugated backbone, thus favoring a pinning regime for each lateral fragments under

bias. In turn, the latter amplifies the electric field in the junction and promotes a strong polarization effect. The situation is opposite in the fully conjugated closed isomer where the electric field is screened, thus limiting the extent of polarization effects. Introducing metal induced gap states via saturated spacers prevents the pinning of the delocalized orbital and annihilates the amplification of the electric field together with the polarization of the delocalized orbital; most importantly, this translates into a preservation of the transmission peak intensity under bias.

These results relying on the concepts of chemical potential equalization and metal induced gap states (MIGS) bring important new guidelines for the design of functional molecular junctions. The relationship established between pinning and polarization effects, with the accompanied significant impact on the transmission spectrum, has in particular strong implications for the design of molecular rectifiers. We finally stress that the consideration of the orbitals of the molecule perturbed by gold atoms rather than those of the isolated compounds is absolutely required to set these principles at work.

Supporting Information

Supporting Information is available from the Wiley Online Library or from the author.

Acknowledgements

This work has been supported by the European project ONE-P (NMP3LA-2008–212311), the Interuniversity Attraction Poles Programme (P7/05) initiated by the Belgian Science Policy Office, and the Belgian National Fund for Scientific Research (FRS-FNRS). C.V.D. and J.C. are FNRS research fellows.

Received: March 12, 2014
Revised: May 12, 2014
Published online: August 5, 2014

[1] a) A. Aviram, *Adv. Mater.* **1989**, *1*, 124; b) K. S. Kwok, J. C. Ellenbogen, *Mater. Today* **2002**, *5*, 28; c) M. A. Ratner, *Mater. Today* **2002**, *5*, 20; d) J. R. Heath, M. A. Ratner, *Phys. Today* **2003**, *56*, 43.
[2] E. Scheer, J.-C. Cuevas, *Molecular Electronics: An Introduction to Theory and Experiment*, World Scientific Publishing Company, Singapore **2010**.
[3] A. Aviram, M. A. Ratner, *Chem. Phys. Lett.* **1974**, *29*, 277.
[4] A. Salomon, D. Cahen, S. Lindsay, J. Tomfohr, V. B. Engelkes, C. D. Frisbie, *Adv. Mater.* **2003**, *15*, 1881.
[5] a) R. L. McCreery, *Chem. Mater.* **2004**, *16*, 4477; b) D. M. Adams, L. Brus, C. E. D. Chidsey, S. Creager, C. Creutz, C. R. Kagan, P. V. Kamat, M. Lieberman, S. Lindsay, R. A. Marcus, R. M. Metzger, M. E. Michel-Beyerle, J. R. Miller, M. D. Newton, D. R. Rolison, O. Sankey, K. S. Schanze, J. Yardley, X. Zhu, *J. Phys. Chem. B* **2003**, *107*, 6668.
[6] S. M. Lindsay, M. A. Ratner, *Adv. Mater.* **2007**, *19*, 23.
[7] R. L. McCreery, H. Yan, A. J. Bergren, *Phys. Chem. Chem. Phys.* **2013**, *15*, 1065.
[8] Y. Imry, R. Landauer, *Rev. Mod. Phys.* **1999**, *71*, S306.
[9] a) M. Brandbyge, J.-L. Mozos, P. Ordejón, J. Taylor, K. Stokbro, *Phys. Rev. B* **2002**, *65*, 165401; b) K. Stokbro, J. Taylor, M. Brandbyge, H. Guo, in *Introducing Molecular Electronics* Vol. *680* (Eds: G. Cuniberti, K. Richter, G. Fagas), Springer Berlin Heidelberg **2005**, 117.
[10] J. Taylor, H. Guo, J. Wang, *Phys. Rev. B* **2001**, *63*, 245407.
[11] a) Y. Xue, S. Datta, M. A. Ratner, *Chem. Phys.* **2002**, *281*, 151; b) M. Koentopp, C. Chang, K. Burke, R. Car, *J. Phys.: Condens. Matter* **2008**, *20*, 083203; c) L. A. Zotti, T. Kirchner, J.-C. Cuevas, F. Pauly, T. Huhn, E. Scheer, A. Erbe, *Small* **2010**, *6*, 1529.
[12] a) B. Kim, S. H. Choi, X. Y. Zhu, C. D. Frisbie, *J. Am. Chem. Soc.* **2011**, *133*, 19864; b) H. Sakaguchi, A. Hirai, F. Iwata, A. Sasaki, T. Nagamura, E. Kawata, S. Nakabayashi, *Appl. Phys. Lett.* **2001**, *79*, 3708; c) N. J. Tao, *Nat. Nanotechnol.* **2006**, *1*, 173.
[13] J. P. Bergfield, M. A. Ratner, *Phys. Status Solidi B* **2013**, *250*, 2249.
[14] F. Meng, Y.-M. Hervault, L. Norel, K. Costuas, C. Van Dyck, V. Geskin, J. Cornil, H. H. Hng, S. Rigaut, X. Chen, *Chem. Sci.* **2012**, *3*, 3113.
[15] C. Van Dyck, V. Geskin, A. J. Kronemeijer, D. M. de Leeuw, J. Cornil, *Phys. Chem. Chem. Phys.* **2013**, *15*, 4392.
[16] M. Irie, *Chem. Rev.* **2000**, *100*, 1685.
[17] a) D. Dulić, S. J. van der Molen, T. Kudernac, H. T. Jonkman, J. J. D. de Jong, T. N. Bowden, J. van Esch, B. L. Feringa, B. J. van Wees, *Phys. Rev. Lett.* **2003**, *91*, 207402; b) H. Jin, C. Fan, A. L. Paul, A. Joakim, D. S. Stephen, G. Devens, A. M. Thomas, L. M. Ana, L. Jun, F. S. Otto, M. L. Stuart, *Nanotechnology* **2005**, *16*, 695; c) A. J. Kronemeijer, H. B. Akkerman, T. Kudernac, B. J. van Wees, B. L. Feringa, P. W. M. Blom, B. de Boer, *Adv. Mater.* **2008**, *20*, 1467; d) S. J. van der Molen, J. Liao, T. Kudernac, J. S. Agustsson, L. Bernard, M. Calame, B. J. van Wees, B. L. Feringa, C. Schönenberger, *Nano Lett.* **2008**, *9*, 76.
[18] J. Tersoff, *Phys. Rev. Lett.* **1984**, *52*, 465.
[19] R. T. Tung, *Mater. Sci. Eng.: R: Rep.* **2001**, *35*, 1.
[20] a) M. Fahlman, A. Crispin, X. Crispin, S. K. M. Henze, M. P. d. Jong, W. Osikowicz, C. Tengstedt, W. R. Salaneck, *J. Phys.: Condens. Matter* **2007**, *19*, 183202; b) S. Braun, W. R. Salaneck, M. Fahlman, *Adv. Mater.* **2009**, *21*, 1450; c) J. Hwang, A. Wan, A. Kahn, *Mater. Sci. Eng.: R: Rep.* **2009**, *64*, 1.
[21] a) M. Levy, J. P. Perdew, V. Sahni, *Phys. Rev. A* **1984**, *30*, 2745; b) C. O. Almbladh, U. von Barth, *Phys. Rev. B* **1985**, *31*, 3231.
[22] a) G. Heimel, F. Rissner, E. Zojer, *Adv. Mater.* **2010**, *22*, 2494; b) G. Heimel, E. Zojer, L. Romaner, J.-L. Brédas, F. Stellacci, *Nano Lett.* **2009**, *9*, 2559; c) F. Rissner, G. M. Rangger, O. T. Hofmann, A. M. Track, G. Heimel, E. Zojer, *ACS Nano* **2009**, *3*, 3513.
[23] a) A. Staykov, D. Nozaki, K. Yoshizawa, *J. Phys. Chem. C* **2007**, *111*, 3517; b) A. Odell, A. Delin, B. Johansson, I. Rungger, S. Sanvito, *ACS Nano* **2010**, *4*, 2635; c) C. D. Pemmaraju, I. Rungger, S. Sanvito, *Phys. Rev. B* **2009**, *80*, 104422.
[24] M. J. T. Frisch, G. W. Schlegel, H. B. Scuseria, G. E. Robb, M. A. Cheeseman, J. R. Scalmani, G. Barone, V. Mennucci, B. Petersson, G. A. Nakatsuji, H. Caricato, M. Li, X. Hratchian, H. P. Izmaylov, A. F. Bloino, J. Zheng, G. Sonnenberg, J. L. Hada, M. Ehara, M. Toyota, K. Fukuda, R. Hasegawa, J. Ishida, M. Nakajima, T. Honda, Y. Kitao, O. Nakai, H. Vreven, T. Montgomery, J. A. Peralta Jr., J. E. Ogliaro, F. Bearpark, M. Heyd, J. J. Brothers, E. Kudin, K. N. Staroverov, V. N. Kobayashi, R. Normand, J. Raghavachari, K. Rendell, A. Burant, J. C. Iyengar, S. S. Tomasi, J. Cossi, M. Rega, N. Millam, N. J. Klene, M. Knox, J. E. Cross, J. B. Bakken, V. Adamo, C. Jaramillo, J. Gomperts, R. Stratmann, R. E. Yazyev, O. Austin, A. J. Cammi, R. Pomelli, C. Ochterski, J. W. Martin, R. L. Morokuma, K. Zakrzewski, V. G. Voth, G. A. Salvador, P. Dannenberg, J. J. Dapprich, S. Daniels, A. D. Farkas, Ö. Foresman, J. B. Ortiz, J. V. Cioslowski, J. Fox, D. J., Gaussian, Inc., Wallingford CT, **2009**.
[25] a) A. D. Becke, *J. Chem. Phys.* **1993**, *98*, 5648; b) A. D. Becke, *Phys. Rev. A* **1988**, *38*, 3098; c) C. Lee, W. Yang, R. G. Parr, *Phys. Rev. B* **1988**, *37*, 785.
[26] a) A. Goldberg, A. Murakami, K. Kanda, T. Kobayashi, S. Nakamura, K. Uchida, H. Sekiya, T. Fukaminato, T. Kawai, S. Kobatake, M. Irie, *J. Phys. Chem. A* **2003**, *107*, 4982; b) F. L. E. Jakobsson, P. Marsal,

S. Braun, M. Fahlman, M. Berggren, J. r. m. Cornil, X. Crispin, *J. Phys. Chem. C* **2009**, *113*, 18396.

[27] a) J. P. Perdew, K. Burke, M. Ernzerhof, *Phys. Rev. Lett.* **1996**, *77*, 3865; b) Y. Zhang, W. Yang, *Phys. Rev. Lett.* **1998**, *80*, 890.

[28] J. Junquera, Ó. Paz, D. Sánchez-Portal, E. Artacho, *Phys. Rev. B* **2001**, *64*, 235111.

[29] a) H. Kondoh, M. Iwasaki, T. Shimada, K. Amemiya, T. Yokoyama, T. Ohta, M. Shimomura, S. Kono, *Phys. Rev. Lett.* **2003**, *90*, 066102; b) F. Remacle, R. D. Levine, *Chem. Phys. Lett.* **2004**, *383*, 537; c) A. Perrier, F. Maurel, J. Aubard, *J. Phys. Chem. A* **2007**, *111*, 9688.

[30] a) J. Li, G. Speyer, O. F. Sankey, *Phys. Rev. Lett.* **2004**, *93*, 248302; c) D. Q. Andrews, R. Cohen, R. P. Van Duyne, M. A. Ratner, *J. Chem. Phys.* **2006**, *125*, 174718; c) X.-W. Yan, R.-J. Liu, Z.-L. Li, B. Zou, X.-N. Song, C.-K. Wang, *Chem. Phys. Lett.* **2006**, *429*, 225.

[31] H. J. Monkhorst, J. D. Pack, *Phys. Rev. B* **1976**, *13*, 5188.

[32] a) R. Stowasser, R. Hoffmann, *J. Am. Chem. Soc.* **1999**, *121*, 3414; b) E. J. Baerends, O. V. Gritsenko, R. van Meer, *Phys. Chem. Chem. Phys.* **2013**, *15*, 16408.

[33] H. Mera, Y. M. Niquet, *Phys. Rev. Lett.* **2010**, *105*, 216408.

[34] C. Jin, M. Strange, T. Markussen, G. C. Solomon, K. S. Thygesen, *J. Chem. Phys.* **2013**, *139*, 184307.

[35] M. Strange, C. Rostgaard, H. Häkkinen, K. S. Thygesen, *Phys. Rev. B* **2011**, *83*, 115108.

[36] a) A. Cehovin, H. Mera, J. H. Jensen, K. Stokbro, T. B. Pedersen, *Phys. Rev. B* **2008**, *77*, 195432; a) S.-H. Ke, H. U. Baranger, W. Yang, *J. Chem. Phys.* **2007**, *126*, 201102.

[37] a) J. B. Neaton, M. S. Hybertsen, S. G. Louie, *Phys. Rev. Lett.* **2006**, *97*, 216405; b) J. M. Garcia-Lastra, K. S. Thygesen, *Phys. Rev. Lett.* **2011**, *106*, 187402; c) A. M. Souza, I. Rungger, C. D. Pemmaraju, U. Schwingenschloegl, S. Sanvito, *Phys. Rev. B* **2013**, *88*, 165112; d) Q. Wu, T. Van Voorhis, *J. Chem. Phys.* **2006**, *125*, 164105.

[38] J. M. Garcia-Lastra, C. Rostgaard, A. Rubio, K. S. Thygesen, *Phys. Rev. B* **2009**, *80*, 245427.

[39] R. G. Parr, W. Yang, *Density-Functional Theory of Atoms and Molecules,*Oxford University Press, New York **1989**.

[40] L. Venkataraman, Y. S. Park, A. C. Whalley, C. Nuckolls, M. S. Hybertsen, M. L. Steigerwald, *Nano Lett.* **2007**, *7*, 502.

[41] N. Crivillers, A. Liscio, F. Di Stasio, C. Van Dyck, S. Osella, D. Cornil, S. Mian, G. M. Lazzerini, O. Fenwick, E. Orgiu, F. Reinders, S. Braun, M. Fahlman, M. Mayor, J. Cornil, V. Palermo, F. Cacialli, P. Samori, *Phys. Chem. Chem. Phys.* **2011**, *13*, 14302.

[42] R. S. Mulliken, *J. Chem. Phys.* **1934**, *2*, 782.

[43] R. G. Parr, R. A. Donnelly, M. Levy, W. E. Palke, *J. Chem. Phys.* **1978**, *68*, 3801.

[44] R. T. Sanderson, *Science* **1951**, *114*, 670.

[45] W. J. Mortier, S. K. Ghosh, S. Shankar, *J. Am. Chem. Soc.* **1986**, *108*, 4315.

[46] a) R. T. Tung, *Phys. Rev. B* **2001**, *64*, 205310; b) X. Crispin, V. Geskin, A. Crispin, J. Cornil, R. Lazzaroni, W. R. Salaneck, J.-L. Brédas, *J. Am. Chem. Soc.* **2002**, *124*, 8131.

[47] G. Kastlunger, R. Stadler, in *http://arxiv.org/abs/1312.5607*, **2013**.

[48] a) G. C. Liang, A. W. Ghosh, M. Paulsson, S. Datta, *Phys. Rev. B* **2004**, *69*, 115302; b) H. Dalgleish, G. Kirczenow, *Phys. Rev. B* **2006**, *73*, 245431; c) Y. Xue, M. A. Ratner, *Phys. Rev. B* **2003**, *68*, 115406; d) C.-C. Kaun, H. Guo, *Nano Lett.* **2003**, *3*, 1521; e) Ž. Crljen, A. Grigoriev, G. Wendin, K. Stokbro, *Phys. Rev. B* **2005**, *71*, 165316; f) Y. X. Zhou, F. Jiang, H. Chen, R. Note, H. Mizuseki, Y. Kawazoe, *J. Chem. Phys.* **2008**, *128*, 044704.

[49] a) C. Zeng, B. Li, B. Wang, H. Wang, K. Wang, J. Yang, J. G. Hou, Q. Zhu, *J. Chem. Phys.* **2002**, *117*, 851; b) J. A. Malen, P. Doak, K. Baheti, T. D. Tilley, R. A. Segalman, A. Majumdar, *Nano Lett.* **2009**, *9*, 1164.